RESEARCH PAPER

Revision of TD1 and TD2 stratigraphic sequence of Gran Dolina cave (Sierra de Atapuerca, Spain)

I. Campaña[1] · A. Benito-Calvo[2] · A. Pérez-González[3] · A. Álvaro-Gallo[2] · L. Miguens-Rodríguez[2] ·
J. Iglesias-Cibanal[2] · J. M. Bermúdez de Castro[2] · E. Carbonell[4]

Abstract

Gran Dolina is a cavity infilled by at least 25 m of Pleistocene sediments divided into 12 lithostratigraphic units and 19 sedimentary facies. These sedimentary facies have been divided into allochthonous facies, defined as sediment inputs from the outside, and autochthonous facies, defined as sediments generated within the karst; but this division has been challenged in recent works. In this study, TD1 and TD2 units of Gran Dolina have been detailed studied and the use of autochthonous facies has been assessed. For that purpose, we have studied the stratigraphic excavation profile, combining field observation with laboratory sedimentary analysis (sieving, laser diffraction, and XRD) to characterize the texture and structure of the sediments. Based on these studies, a total of 8 sedimentary facies have been identified. Consequently, TD1 unit has been separated into two sub-units and 13 layers, while the TD2 unit has been divided into three sub-units. The facies associations indicate a succession of phreatic and vadose phases that would define together epiphreatic conditions inside the cave, related to the transition between Arlanzón valley terraces T3 and T4. Interior facies (and entrance facies for allochthonous facies) is proposed to define Gran Dolina's sediments since the facies analyses indicate transport by underground flows.

Keywords Early Pleistocene · Atapuerca · Cave sedimentation · Sedimentary facies · Interior facies

Resumen

Gran Dolina es una cueva rellena por al menos 25 m de sedimentos pleistocenos dividido en 12 unidades litoestratigráficas y 19 facies sedimentarias. Estas facies sedimentarias se han dividido entre facies alóctonas, definidas como entradas de sedimentos desde el exterior, y facies autóctonas, definidas como sedimentos generadas dentro del karst; sin embargo, esta clasificación de facies ha sido cuestionada en trabajos recientes. En este estudio se ha descrito en detalle las unidades TD1 y TD2 de Gran Dolina y se ha evaluado la idoneidad del uso de facies autóctonas. Para ello, se ha estudiado la sección estratigráfica de la excavación arqueológica, combinando observaciones de campo con análisis de laboratorio (tamizado, difracción láser y DRX) para caracterizar la textura y estructura de los sedimentos. A partir de estos estudios, se han identificado un total de 8 facies sedimentarias, y se han separado la unidad TD1 en dos sub-unidades y 13 niveles, y la unidad TD2 en tres sub-unidades. La asociación de facies indica una sucesión de fases freáticas y vadosas que definiría conjuntamente condiciones epifreáticas en el interior de la cueva, relacionadas con la transición entre la terraza T3 y la terraza T4 del valle del río Arlanzón. Por tanto, se propone el término facies de interior (y facies de entrada en vez de facies alóctonas) para definir los sedimentos de las unidades de TD1 y TD2 de Gran Dolina, ya que el análisis de facies indica transporte de los sedimentos por corrientes subterráneas.

Palabras clave Pleistoceno inferior · Atapuerca · Sedimentación en Cueva · Facies sedimentarias · Facies de interior

✉ I. Campaña
   i.campanna.lozano@gmail.com

1 Departamento de Ecología y Geología, Facultad de Ciencias, Universidad de Málaga, Campo de Teatinos S/N, 29071 Málaga, Spain

2 Centro Nacional de Investigación Sobre Evolución Humana (CENIEH), Paseo de La Sierra de Atapuerca 3, 09002 Burgos, Spain

3 Instituto de Evolución en Africa-IDEA, Covarrubias 36, 28010 Madrid, Spain

4 Departament d'Història i Història de l'Art, Universitat Rovira i Virgili, Avinguda de Catalunya 35, 43002 Tarragona, Spain

1 Introduction

Caves are natural traps that can preserve sediments and archaeological remains from outside erosion. Sedimentary infills have been well studied in many caves since the end of the XIX century until now (Arriolabengoa et al., 2015; Bonifay, 1956; Bull, 1981; Cooke, 1938; Farrand et al., 2001; Kadlec et al., 2008; Kampolis et al., 2022; Martini et al., 2021; Ossowski, 1882; Shaw, 1992, among others), providing data about the processes of formation and the relationship between the caves and their environment. Classification of cave deposits traditionally divides cave sedimentary facies into three main groups: allochthonous, autochthonous, and chemical deposits (Ford & Williams, 2007; White, 2007).

Allochthonous sediments are sediment inputs from the outside. These sediments enter the cave from near entrances and can accumulate through different sedimentary processes such as gravity (e.g. debris fall, debris flow, mudflow), fluvial (floodplain and channels), or aeolian agents. In contrast, autochthonous sediments are generated within the karst, resulting from cave processes such as weathering or breakdown. These kinds of sediment are usually produced when the cave is closed to the outside, preventing autochthonous sediment accumulation. Although, at some times, autochthonous facies can produce in open caves or rock shelters, as breakdowns

(Martini et al., 2018). Chemical deposits are mineral growths that are produced inside the caves. The most known are calcite speleothem, but also, they can be evaporites, phosphates, or even ice. These usually are very slow growth deposits that need a closed environment.

Gran Dolina cave is situated in the Sierra de Atapuerca (Burgos, Spain) (Fig. 1). It has a 25 m thick sedimentary infill that has provided a significant amount of archaeological and paleontological remains documenting human activity and environment during the last million years (Carbonell et al., 2008; Ortega et al., 2014; Rodríguez et al., 2011). The sediment of Gran Dolina has been separated into 12 main lithostratigraphic units, with a total of 19 sedimentary facies identified so far (Fig. 2, Table 1). The 12 lithostratigraphic units were named TD1–TD8, TD8-9, and TD9–TD11 from bottom to top (Gil et al., 1987; Parés & Pérez-González, 1999; Fig. 2). In these classifications, units were defined following allostratigraphic criteria based mainly on fieldwork observations. TD1 and TD2 were defined as autochthonous sediments, whereas TD3 to TD11 were defined as allochthonous sediments (Campaña et al., 2017). The TD3 unit is not present because it was totally excavated in the nineties. Allochthonous sediments include two remarkable archeo-paleontological units: the TD6 unit that yields human remains, stone tools and fauna dated to about 0.8–0.9 Ma (Berger et al., 2008; Carbonell et al., 1999; Duval et al., 2018; Gómez-Olivencia et al.,
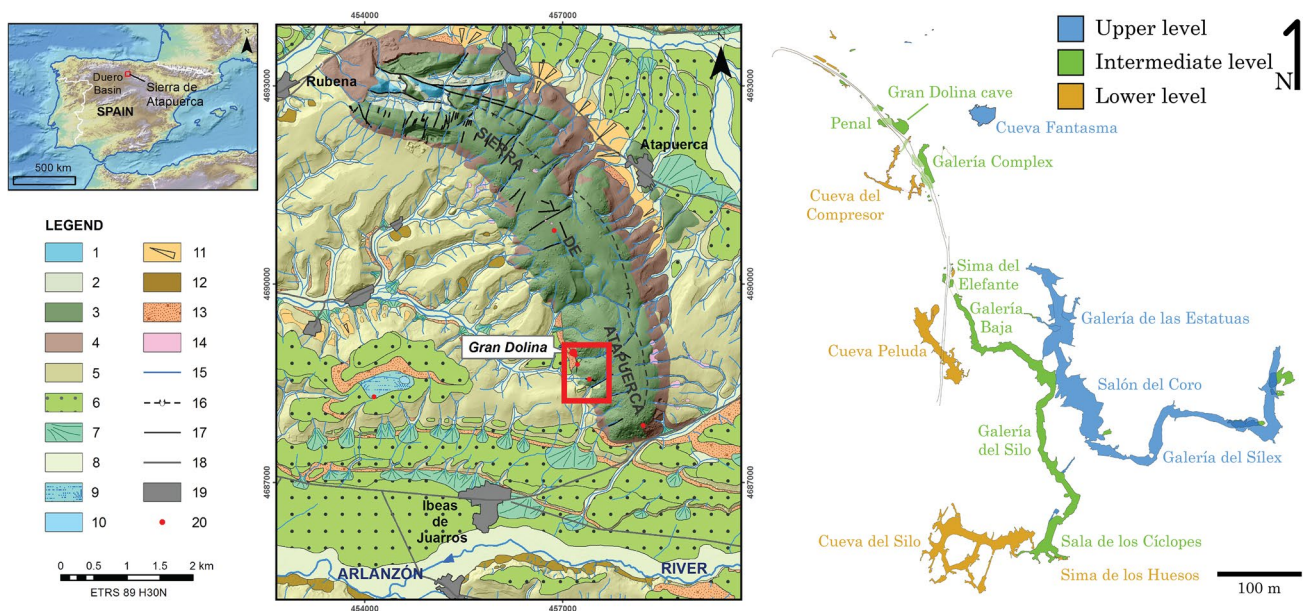

Fig. 1 General location, geological map of the Sierra de Atapuerca (simplified from Benito-Calvo & Pérez-González, 2015) and map of the Atapuerca multilevel cave system (modified from Ortega et al., 2013). The underground karstic infills of the Railway Trench are pale green (Bermejo et al., 2020). Legend: 1, Jurassic; 2, Early Cre-

taceous; 3, Late Cretaceous; 4, Oligocene; 5, Miocene; 6, Fluvial terraces; 7, Cones; 8, Floodplains and valley floors; 9, Semi-endorheic areas; 10, Seasonal pools; 11, Glacis; 12, Landslides; 13, Colluvium; 14, Dolina floors; 15, Drainage network; 16, Inferred overturned anticline; 17, Faults; 18, Roads; 19, Urban areas; 20, Archaeological sites
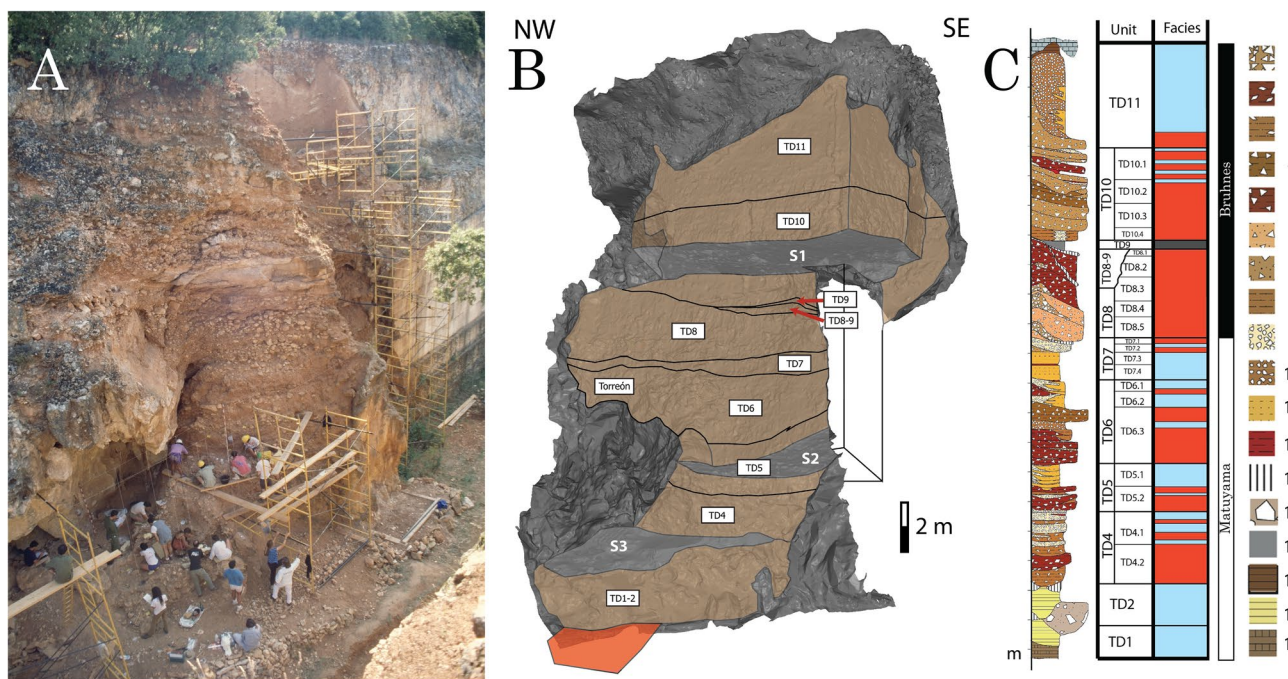
Fig. 2 **A** Gran Dolina site in 1994 (M. A. Martín). **B** 3D model of the Gran Dolina site in 2012. Brown areas indicate stratigraphic units. Grey areas are the wall and roof of the cave. The red area is the current situation of the TD1 and TD2 test pit. **C** Stratigraphic column of Gran Dolina site (Campaña et al., 2017). Legend Sedimentary facies: 1, Debris fall; 2, Debris flow facies A; 3, Debris flow facies B; 4, Debris flow facies C; 5, Debris flow facies D; 6, Debris flow facies E; 7, Debris flow facies F; 8, Mud flow; 9, Channel facies A; 10, Channel facies B; 11, Floodplain; 12, Decantation; 13, Speleothem; 14, Breakdown; 15, Phosphatic accumulation; 16, Weathering detritus; 17, Autochthonous fluvial facies A; 18, Autochthonous fluvial facies B. Campaña et al., (2017) for a detailed description of these facies

Table 1 Classification of Sedimentary facies described in Gran Dolina cave (Campaña et al., 2017)

Allochthonous facies		
Sediment gravity flow	Debris fall	
	Debris flow	DF A
		DF B
		DF C
		DF D
		DF E
		DF F
	Mud flow	
Fluvial flow	Channel	CH A
		CH B
	Floodplain	
	Decantation	
Autochthonous facies		
Speleothem		
Breakdown		
Phosphatic accumulation		
Weathering detritus		
Fluvial		FL A
		FL B
		FL C

2012; Pablos et al., 2012; Parés et al., 2013; Rodríguez-Gómez et al., 2013), and the TD10 unit that includes two rich layers of stone tools and fauna interpreted as a human campsite dated to about 0.35 Ma (Falguères et al., 1999, 2013; Moreno et al., 2015; Ollé et al., 2013).

During the excavation of 2013, a vertical test pit in the NW section was started at the base of the Gran Dolina site (Fig. 3) to reach the cave's floor. It was reached at seven meters depth, showing a total of nine meters of the sedimentary sequence of sterile sediments mainly composed of sand, silt, and clay. After, a borehole was drilled in the Railway Trench next to the Gran Dolina site revealing 10-m thick sediment fill composed of silts and clays (Bermejo et al., 2020). These sediments were included in the TD1 and TD2 units of Gran Dolina, defined as autochthonous facies (Campaña et al., 2017) following the definition of White (2007) and Ford and Williams (2007), and previous works in Sierra de Atapuerca sites (Pérez-González et al., 1995, 1999). The assignment of these sediments to autochthonous facies was due to comparison with the clastic sediments of Gran Dolina, defined as allochthonous facies, and because the Sierra de Atapuerca karst was less understood. The use of this terminology has been challenged since a possible fluvial origin for TD1 and TD2 has been previously postulated by different studies based on sedimentology (Campaña,
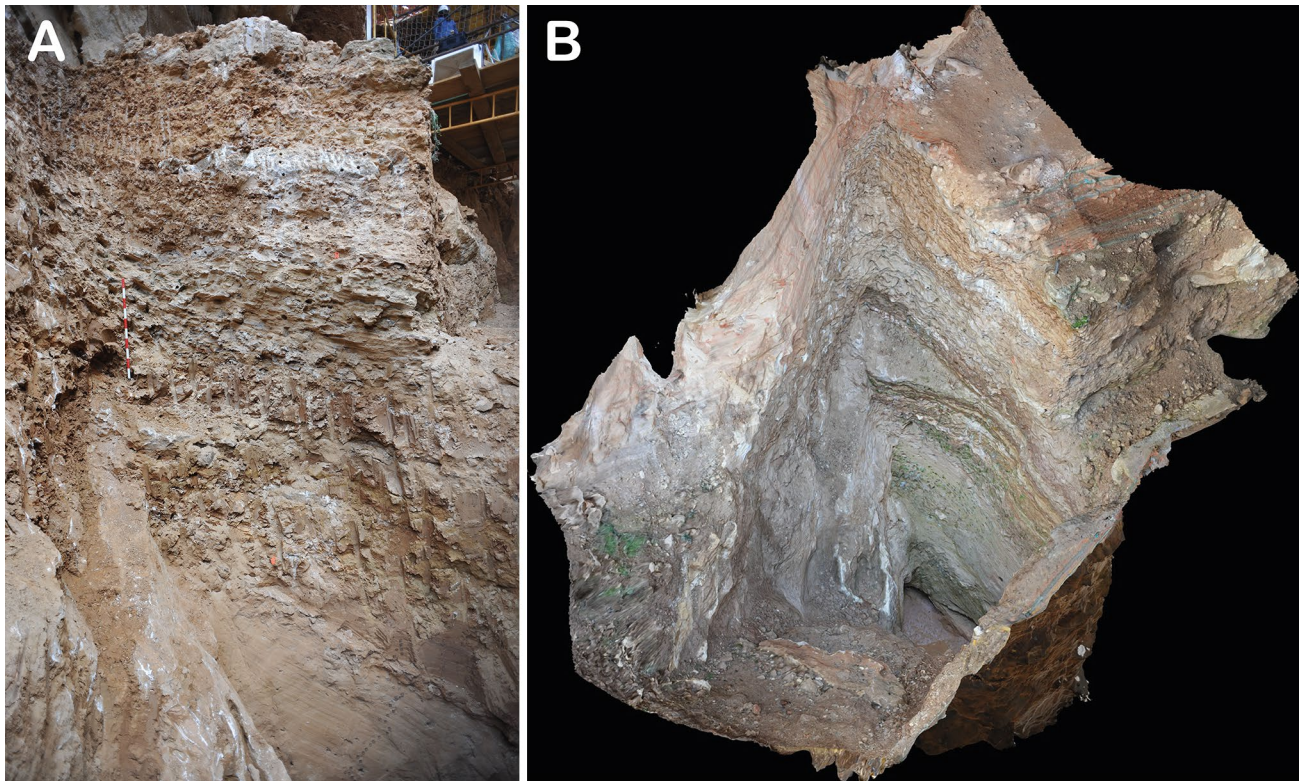
Fig. 3 Vertical test pit at the base of Gran Dolina cave, where the TD1 and TD2 section was excavated. **A** Image of TD1 and TD2 section. **B** Top view of 3D model of TD1 and TD2 made by photogrammetry

2018), particle shape analyses (Campaña et al., 2016), and geochronology (Duval et al., 2022; Parés et al., 2018).

Although TD1 and TD2 are sterile lithostratigraphic units, their study is necessary to understand the evolution of the karst system, providing key information about the formation and sedimentation processes in the cavities during the persistence of water table conditions related to fluvial phreatic levels. The formation of the middle level of the karst, where Gran Dolina cave belongs, was related to the terrace T3 of the Arlanzón River (Benito-Calvo et al., 2017), which was dated by ESR to 1.14 ± 0.13 Ma (Moreno et al., 2012). Recently, TD1 and TD2 have been dated by Electron Spin Resonance (ESR) and single-grain thermally transferred optically stimulated luminescence (SG TT-OSL) methods applied to quartz grains, in combination with magnetostratigraphy, constraining these units to between ~ 1.4 Ma and ~ 0.9 Ma (Duval et al., 2022; Parés et al., 2018). This chronology means that the sedimentary deposit of Gran Dolina cavity started quickly after its formation. Therefore the study of these sediments can indicate the evolution of the environment during the Early Pleistocene, at a time when other caves in the karstic system already had sediments from outside, such as Sima

del Elefante (Rosas et al., 2006), and the oldest hominins from West Europe were living in the Sierra de Atapuerca (Carbonell et al., 2008).

This work aims to understand the cave dynamic and hydric regime within Gran Dolina cave during the period of sedimentation of TD1 and TD2, as well as its relationship with the rest of the karst and the hydrographic basin. To reach this aim, the first detailed description and interpretation of the TD1 and TD2 stratigraphic units is needed, with particular emphasis on sedimentary processes and sediment provenance.

2 Geologic context

The Gran Dolina site is situated in the south of the Sierra de Atapuerca in central Spain (N42° 21′ 05.29″; W3° 30′ 39.20″; WGS84) (Fig. 1). The Sierra de Atapuerca is a NNW-SSE trending anticlinal ridge belonging to the most north-western outcrop of the Iberian Chain and is situated in the NE Neogene Duero Basin (Benito-Calvo & Pérez-González, 2015). This anticlinal ridge was folded during the Oligocene-Lower Miocene, and it is mainly formed by late Cretaceous limestones and dolostones. This

deformation caused the deposit of syn-orogenic conglomerates, sandstones, and mudstones.

In the Late Miocene-Pliocene, the Duero Basin was opened to the Atlantic Ocean, finalizing the endorheic phase and starting the incision fluvial network of the sediments. During the Quaternary, the main fluvial courses around the Sierra de Atapuerca is the Arlanzón River, and its tributaries the Vena and Pico rivers. The studies of the evolution of these rivers identified a terrace sequence of 14 levels (Benito-Calvo & Pérez-González, 2015; Benito-Calvo et al., 2008; Zazo et al., 1987) that was dated from the Early Pleistocene to the Holocene (Benito-Calvo et al., 2017). Terraces T1 (+92–97 m) to T4 (+60–65 m) have been constrained to the Early Pleistocene, while T5 (+50–58 m) to T11 (+12–14 m) and T12 (+10–11 m) to T13 (+5 m) have been correlated to the Middle and Late Pleistocene, respectively. Finally, T14 (+2–3 m) was tentatively attributed to the Holocene (Benito-Calvo & Pérez-González, 2015; Moreno et al., 2012). The chronologies suggest a putative correlation between terrace deposits and cold Marine Isotope Stages and have allowed reconstruction of the incision rate evolution of the main valley (Benito-Calvo et al., 2017, 2018).

In the Early and Middle Pleistocene, a multilevel endokarst system developed in the Late Cretaceous limestones and dolostones. This karst system consists of 4.7 km of explored passages (Martín-Merino et al., 1981), composed mainly of three levels of subhorizontal water-table controlled galleries (Ortega, 2009; Ortega et al., 2013). These levels appear spatially and chronologically related to some of the Arlanzón fluvial terraces (Benito-Calvo & Pérez-González, 2015; Benito-Calvo et al., 2018; Ortega et al., 2013, 2014; Parés et al., 2015). The karst passages developed during the relatively short period corresponding to terrace aggradation, while vadose entrenchments are related to prolonged incision phases of the Arlanzón River (Benito-Calvo et al., 2018). During the formation of the karst, the Arlanzón waters entered the galleries; they passed through the interior of the karst and left at springs in the Pico Valley headwaters (Ortega et al., 2013).

The upper level developed in a position similar to the base levels associated with the Lower Páramo limestones and the fluvial terrace T2 (+82–86 m) (Ortega et al., 2013), which occur at a similar elevation near the Sierra de Atapuerca (Benito-Calvo & Pérez-González, 2015). It is more than 600 m long with ceilings at 1015–1022 m in altitude, with some vertical chimneys reaching 1030 m in altitude (Ortega et al., 2018). This level is composed by Galería del Sílex, El Portalón, Salón del Coro and Galería de las Estatuas (Fig. 1). The Salón del Coro is the biggest cavity of the Sierra de Atapuerca karst since it includes the three levels. The sediments in this level are mostly composed of clay and silt (Ortega, 2009).

The middle level, where the Gran Dolina cavity is located, is a sinuous subhorizontal phreatic passage about 700 m long and about 1000–1005 m in altitude, associated with the period of stability represented by terrace T3 (+70–78 m) (Ortega et al., 2018), during the Early Pleistocene (Benito-Calvo et al., 2008, 2017; Moreno et al., 2012). The vadose regime in this level was marked by incision of the Arlanzón River between T3 and T4 (+60–65 m) (Benito-Calvo et al., 2017; Ortega et al., 2013). Currently, this level has a subterranean zone formed by Sala de Los Cíclopes, Galería del Silo and Galería Baja (Fig. 1), in addition to other sediment-filled galleries recently discovered (Bermejo, 2021; Bermejo et al., 2017), and another aerial zone cut by a Railway Trench that revealed numerous sedimentary fills and cavities, including three important archaeological sites: Sima del Elefante cave, Galeria-Tres Simas cave and Gran Dolina cave (Ortega et al., 2018). These three caves are sediment-fill caves that preserve important archaeological and paleontological remains (Rodríguez et al., 2011).

The Galería Complex is situated in the south of Gran Dolina and is composed of three sub-sections: Covacha de los Zarpazos to the north, Galería in the centre, and Tres Simas in the south (Ortega, 2009). Covacha de los Zarpazos is about a 15 m length cavity with direction northeast that continues to Galería at the south. Galería is the main subhorizontal conduit of the site. Tres Simas is three vertical shafts connected in their lower part with Galería. The stratigraphic sequence of Galería Complex has 13 m of thickness in the current section, which continues with at least 17 m under the current path (Bermejo et al., 2020); thus the cave has more than 30 m thick of sediments. The Galería sediments have been separated into five litho-stratigraphic units, from the bottom to the top, GI to GV units (Pérez-González et al., 1995, 2001). Matuyama/Brunhes paleomagnetism boundary is observed near the top of the GI unit (Pérez-González et al., 2001), which is formed by similar facies of TD1 and TD2. Meanwhile, the luminescence chronology of GIV shows results of 0.185 ± 0.026 Myr (Berger et al., 2008) and 0.255 ± 0.021 Myr (Demuro et al., 2014).

The Sima del Elefante is a 25 m thick cave sedimentary infill divided into 16 litho-stratigraphic units, called TE7 to TE21, from bottom to top (Huguet et al., 2017; Rosas et al., 2001, 2006). These units were grouped into three sedimentary phases: lower, middle, and upper phases. Sediments composing the Sima del Elefante site are all entrance facies formed by mudflows and debris flows. The lower phase has been dated by cosmogenic to 1.13 ± 0.18 Myr for TE7, and 1.22 ± 0.16 Myr for TE9 (Carbonell et al., 2008). In this site, the Matuyama/Brunhes paleomagnetism boundary is described between TE16 and TE17 units (Parés et al., 2006) according to the faunal associations, TL-IRSL, and cosmogenic dating (Carbonell et al., 2008).

The lower cave level has been correlated to T4 (+ 60–65 m)/T5 (+ 50–54 m) (Ortega et al., 2013). Their ceilings are situated at 990 m.a.s.l with vertical chimneys reaching 994 m in altitude (Ortega et al., 2018). This level is located further west than the upper and middle levels and is formed by Cueva del Silo, Cueva Peluda, Cueva del Compresor and Sala del Caos (Fig. 1). These conducts have a phreatic morphology and are smaller than the cave of the other levels (Ortega et al., 2014).

In the lower level's south, a small karst sub-level was developed. To this sub-level belongs Sima de los Huesos and the lowest area of Cueva del Silo, which has ceilings below 985 m.a.s.l (Ortega, 2009).

3 Materials and methods

3.1 Sedimentological studies

The study and classification of the different facies and sedimentary environments of Gran Dolina required a detailed description of the available stratigraphic excavation profiles. Fieldwork has been combined with laboratory analyses to describe the mineralogy and texture of the sediments. For this, eight samples were taken from non-cemented layers in the stratigraphic section.

Particle size sieving and laser diffraction techniques have been used. For sieving techniques, φ size sieves, ranging from $- 1\varphi$ to 4φ, were used (Geology Laboratory, CENIEH). Larger sizes have not been analyzed because a large amount of sample would have been required to obtain a representative analysis. A Beckman Coulter LS13 320 laser diffraction particle size analyzer was used to measure the silt and clay fraction particle size. Particle size has been classified following Blott and Pye (2012).

The survey of the stratigraphic profiles and facies maps of the sections was performed using 3D laser scanning techniques (Leica C10), total stations, and photogrammetry (Digital Mapping and 3D Analysis Laboratory, CENIEH), which have served to obtain a 3D model of textures with an RGB image of Gran Dolina and the test pit. Ortho-image of TD1 and TD2 was extracted from the 3D model to study the stratigraphic section.

3.2 Mineralogical and chemical analyses

Mineralogical and chemical composition of the bulk samples were obtained by combining two techniques at the Archaeometry laboratory of the CENIEH. The mineralogical phase composition was determined by bulk mineralogy powder X-ray diffractogram (XRD) using a PANalytical X'Pert PRO instrument equipped with a Cu target and a secondary monochromator. The operating conditions for XRD were 45 kV/40 mA in a continuous scan mode performed in the range of 2θ from 3° to 70° with an increment of 0.02°. Semiquantitative analysis was carried out according to the Chung method (Chung, 1975) by using High Score Plus software, based on the Reference Intensity Ratios (RIR) of the existing phases.

Chemical compositions of the major elements were obtained by wavelength dispersive X-ray fluorescence method (XRF) using a PANalytical Axios instrument. For each sample, 0.5 g of bulk grounded material was homogeneously mixed with 5 g of 66:34 mixture of $Li_2B_4O_7$ and $LiBO_2$ flux with LiBr as bead releasing agent. The mixture was then fused to a glass bead in a Pt-Au crucible with a PANalytical Perl'X3 automatic fusion machine. The following elements were measured: SiO_2, Al_2O_3, Fe_2O_3 total, MnO, MgO, CaO, Na_2O, K_2O, TiO_2, P_2O_5, and SO_3. Loss on ignition (LOI) was calculated too.

4 Results

4.1 TD1 and TD2 stratigraphic sequence

TD1 and TD2 stratigraphic units are 8 m thick lithostratigraphic units situated in the base of the 25 m sedimentary infill of the Gran Dolina site (Figs. 2 and 3). TD1 is the lowermost stratigraphic unit lying on the cave floor and topped by a speleothem marking a sedimentary discontinuity with the upper TD2 unit (Fig. 4). The upper discontinuity of TD2 is another speleothem growth, separating this unit from the red clastic sediment of TD4 unit. Based on fieldwork description and textural analyses, TD1 may be divided into two sub-units, comprising thirteen layers, while TD2 consists of three sub-units (Tables 2 and 3, Fig. 4).

4.2 Textural analyses

Textural analyses were carried out on uncemented layers of TD1 and TD2 (Fig. 5). In general, the layers of TD1 and TD2 are composed of millimetric laminations that could not be distinguished during bulk sampling. Therefore, particle size analyses result from both kinds of laminates, a darker laminate and a lighter laminate.

According to the particle size, the sedimentary layers can be divided into sandy layers (TD2.2, TD1.1.6, TD1.2.3, and TD1.2.4), with more than 50% of sand, or silty layers (TD1.1.2, TD1.1.4, TD1.1.8, and TD1.2.2), with more than 45% of silt. The gravels of these samples are limestone clast, surely falling from the ceiling and wall of the cave, and cemented nodules of sand or silt. The sandy layers show a
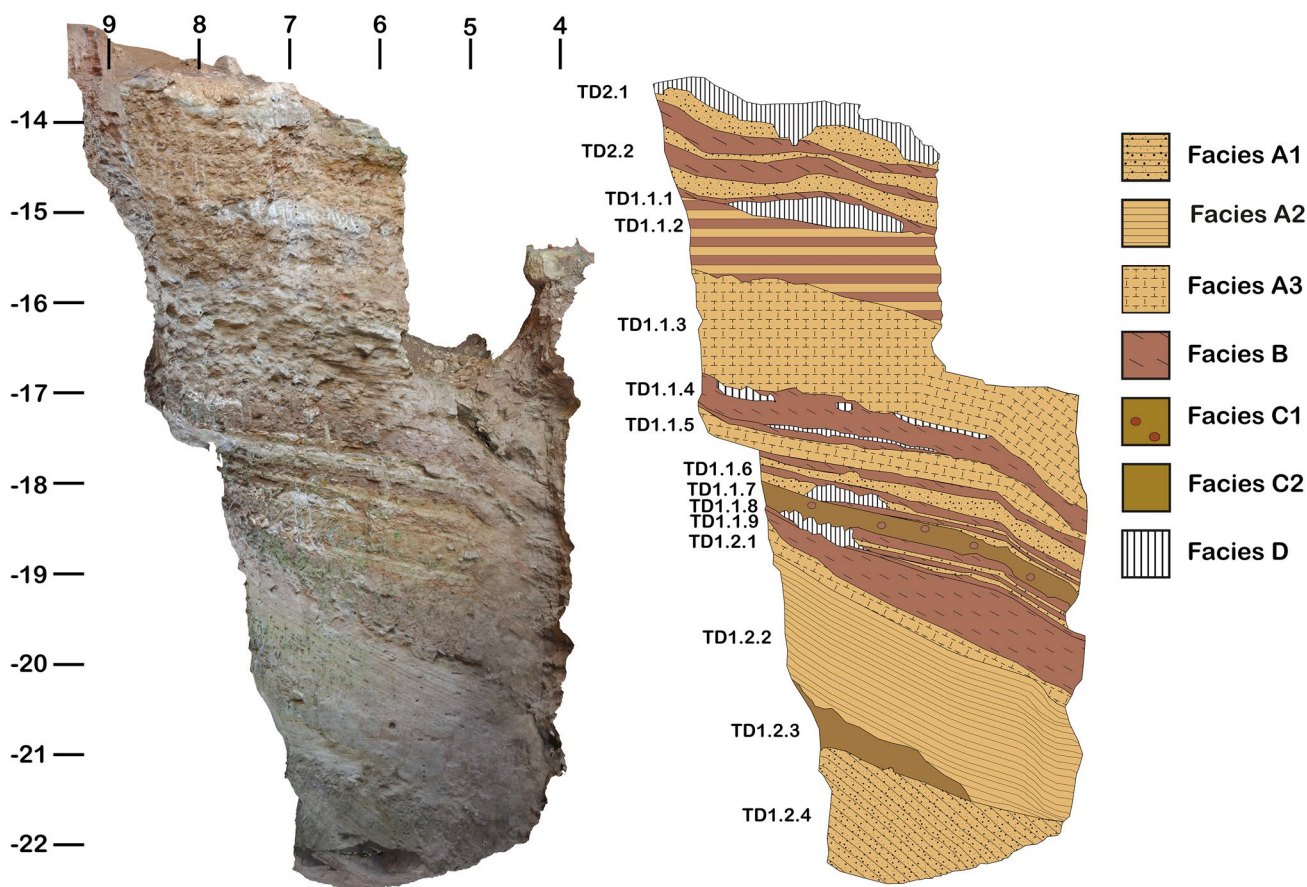
Fig. 4 TD1 and TD2 stratigraphic section from the test pit. A Orthoimage made by photogrammetry. B Sedimentary facies of TD1 and TD2

Table 2 Sedimentary description of the TD1 sub-units and layers

Sub-unit	Layer	Thick	Description
TD1.1	TD1.1.1	30	Speleothem
	TD1.1.2	70	Alternating of laminated 10YR 6/4 light yellowish-brown silt and clayey silt, partially cemented, with clay nodules. Speleothem growth is shown at the top
	TD1.1.3	110	Millimetric lamination of 10YR 6/4 light yellowish-brown clayey silt with cemented sub-layers
	TD1.1.4	45	Millimetric lamination of 5YR 4/4 reddish brown clayey silt with speleothem growth and limestone altered clast on the top
	TD1.1.5	40	A cemented layer of millimetric lamination 10YR 6/4 light yellowish-brown clayey silt
	TD1.1.6	50	Alternating 10YR 7/3 very pale brown silty sand and 5YR 4/4 reddish brown clayey silt, partially cemented and speleothem growth at the north
	TD1.1.7	25	Massive 10YR 5/6 yellowish-brown silty sands with rip-up clasts of red clays, partially cemented
	TD1.1.8	30	Alternating of 10YR 7/3 very pale brown silty sand and 5YR 4/4 reddish brown clayey silt, partially cemented at the north
	TD1.1.9	50	Millimetric lamination of 5YR 4/4 reddish brown clayey silt
TD1.2	TD1.2.1	20	Cemented millimetric lamination of 10YR 6/4 light yellowish-brown silty sand
	TD1.2.2	180	Millimetric lamination of 10YR 6/4 light yellowish-brown silty sand
	TD1.2.3	40	Massive 10YR 5/6 yellowish-brown silty sands
	TD1.2.4	130	Millimetric lamination of 10YR 4/6 dark yellowish-brown silty sand and 5YR 4/4 reddish brown clayed silt

Table 3 Sedimentary description of the TD2 sub-units

Sub-unit	Thick	Description
TD2.1	40	Speleothem
TD2.2	100	Alternating of laminated 10YR 6/4 light yellowish-brown sand and strong yellowish-brown silty sand, partially cemented, with clay nodules
TD2.3	100	One meter diameter limestone clasts from the ceiling and cave walls

similar sand distribution, with medium and fine sand size as predominant (Fig. 5), except for TD1.2.3 which has a very fine sand distribution; meanwhile silty layers have mostly very fine sand. The silt fraction is very similar in all layers, mainly composed of medium and fine silt; except for TD1.1.2, which shows a coarser fraction (Fig. 5). The clay fraction is significant in the layers TD1.1.8 and TD1.2.2, with more than 20% of clay. It is also notable in TD1.1.4, with 17.7% of clay. Considering that this sample has a percentage of gravels that the other samples have not if this percentage of gravels were not considered, TD1.1.4 would have above 20% of clay.

4.3 Mineralogy and chemical analyses

The layers of TD1 and TD2 show a very similar composition, either mineralogy or elemental composition (Tables 4 and 5). The values of the mineralogy are semiquantitative. Quartz, phyllosilicates, and calcite mainly dominate their composition. Quartz seems to be the main mineral of the samples, except in TD1.1.4, which is primarily composed of calcite. This can be due to the high proportion of gravels, either limestone clasts or cemented nodules, in this specific layer.

The elemental analysis shows a clear relation with the mineralogy, with Si as the principal element, except in TD1.1.4, where Ca is the majority due to its richness in calcite. TD1.1.8 has higher values of Al, Fe, and K than the other layers, which can explain by its clay content, which is significantly higher than in the rest of the layers (Fig. 5).

Rutile is only identified in TD2.2, although the result in XRF indicates that TD1.1.2, TD1.1.8, and TD1.2.3 have at least one percent of Ti, suggesting that they also have rutile (Table 5).

4.4 Sedimentary facies

The study of the stratigraphic section of TD1 and TD2 has allowed making a new classification that extends the sedimentary facies classification of Campaña et al., 2017 (Table 1). The layers of TD1 and TD2 have been classified into sedimentary facies based on field observation, particle size analyses, and previous cave sediment classifications

(Campaña et al., 2017; Ford & Williams, 2007; White, 2007). Eight facies have been differentiated and grouped into five main sedimentary facies (Table 6, Figs. 4 and 6).

4.4.1 Facies A

This facies is found at the top of TD1 and TD2, and the bottom of TD1. It consists of millimetric laminated yellowish brown sand and silt with rip-up clasts of silt and clay. The lamination is horizontal, although it is found slightly folded. It is mainly composed of well-sorted quartz, with a few phyllosilicates. No vertical particle size variation is observed in these facies. This facies presents sharp base and top boundaries. Rip-up clasts of other lithology, like clay and silt, are observed, in addition to some layers partially cemented. Depending on its particle size and cementation, three sub-facies have been separated.

4.4.2 Facies A1

Millimetric laminated 10YR 6/4 light yellowish-brown silty sand alternating dark and light laminates. It is composed of more than 50% sand and about 25% silt. This facies is observed in TD2.2 and TD1.2.4, although the last shows a darker Hue.

4.4.3 Facies A2

Millimetric laminated 10YR 6/4 light yellowish brown sandy silt alternating dark and light laminates. It is composed of more than 45% of silt and about 20% of sand. This facies is observed in TD1.1.2 and TD1.2.2.

4.4.4 Facies A3

Millimetric lamination of 10YR 6/4 light yellowish brown silt clays with cemented sub-layers. The cemented layers show, in some cases, thin speleothem growth. This facies is observed in TD1.1.3, TD1.1.5, and TD1.2.1. This millimetric and mostly horizontal lamination corresponds with
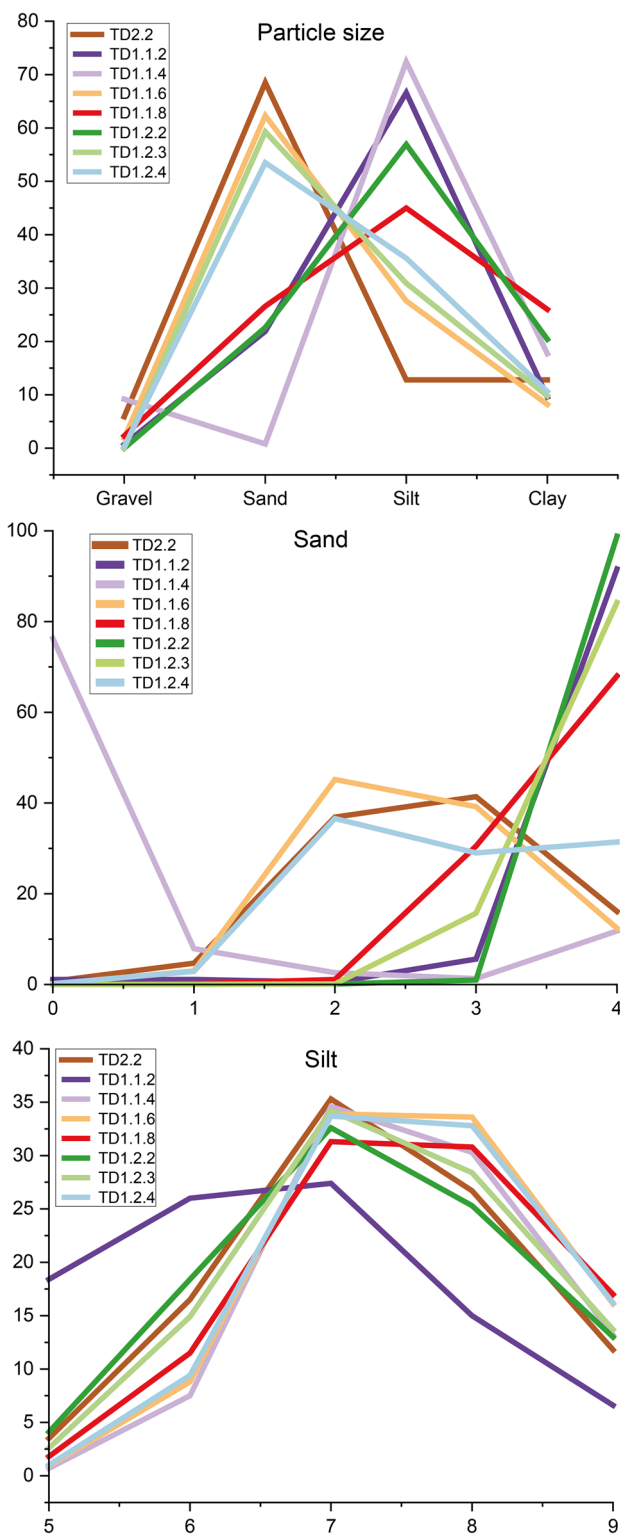
Fig. 5 Particle size distribution of the stratigraphic layers of TD1 and TD2. Axis of abscissa—Phi size

Table 4 Mineralogy of the non-cemented layers of TD1 and TD2 using XRD

Layer	Quartz	Felds	Phyllosilicate	Calcite	Rutile
TD2.2	+++	+	+		+
TD1.1.2	+++	++	+	++	
TD1.1.4	+		+	+++	
TD1.1.6	+++	+	+		
TD1.1.8	+++	+	++	+	
TD1.2.2	+++	+	++	++	
TD1.2.3	+++	+	++	+	
TD1.2.4	+++	+	+		

+++ major phase > 30%, ++ minor phase 30–10%, + traces < 10%

the clay content variation. This facies is comparable to facies FL B of Campaña et al., 2017 (Table 1).

4.4.5 Facies B

Millimetric laminated 5YR 4/4 reddish brown clay and silt. The lamination is tabular, mainly horizontal with slight folds. It is observed in TD2.2, TD1.1.2, TD1.1.4, TD1.1.5, TD1.1.6, TD1.1.8 and TD1.1.9. This facies appears to intercalate by facies A showing sharp boundaries with it.

4.4.6 Facies C

Massive 10YR 5/6 yellowish-brown silty sands. It is composed of more than 50% very fine sand with about 30% silt, and it is observed in TD1.1.7 and TD1.2.3. In TD1.1.7, soft clay and silt nodules are observed. The top and base boundaries are sharps. Two sub-facies are identified.

4.4.7 Facies C1

Massive 10YR 5/6 yellowish-brown silty sands with clay and silt nodules, indicating that eroded previous layers (Fig. 6C). No internal sedimentary structures are observed. It is observed in TD1.1.7.

4.4.8 Facies C2

Massive 10YR 5/6 yellowish-brown silty sands in TD1.2.3. This layer wedges through the West, resting its east side on the wall of the host rock. No internal sedimentary structures are observed.

Table 5 Chemical analysis of the non-cemented layers of TD1 and TD2 using XRF. The results are expressed as oxides weight %

Layer	SiO$_2$	Al$_2$O$_3$	Fe$_2$O$_3$t	MnO	MgO	CaO	Na$_2$O	K$_2$O	TiO$_2$	P$_2$O$_5$	SO$_3$	LOI
TD2.2	86.06	6.50	2.00	0.01	0.40	0.26	0.09	1.52	1.02	0.07	bdl	2.06
TD1.1.2	65.72	8.15	2.86	0.03	0.71	9.62	0.12	1.87	1.00	0.09	bdl	9.81
TD1.1.4	10.04	2.82	1.03	0.03	0.26	47.78	0.07	0.52	0.17	0.05	bdl	37.26
TD1.1.6	89.5	4.25	1.19	0.08	0.30	0.56	0.08	1.03	0.53	0.15	bdl	1.54
TD1.1.8	72.12	12.00	4.35	0.07	0.83	1.96	0.13	2.35	1.02	0.19	bdl	4.98
TD1.2.2	72.45	6.16	2.32	0.02	0.56	7.98	0.11	1.62	0.87	0.08	bdl	7.80
TD1.2.3	82.87	7.19	2.44	0.02	0.51	1.06	0.13	1.88	1.09	0.08	bdl	2.71
TD1.2.4	85.69	6.35	2.79	0.11	0.43	0.22	0.10	1.58	0.81	0.07	bdl	1.85

Table 6 Concise description of the sedimentary facies observed in TD1 and TD2 units

Facies	Sedimentary process	Description
A		
A1	High-energy hydric flow	Millimetric laminated silty sand with rip-up clasts
A2	Medium-energy hydric flow	Millimetric laminated sandy silt with rip-up clasts
A3	Medium-energy hydric flow	Millimetric laminated clayey silt with cemented layers
B	Low-energy hydric flow	Millimetric laminated clayed silt
C		
C1	High-energy hydric flow	Massive silty sands with rip-up clasts
C2	Parallel accretion	Massive silty sands
D	Speleothem	Speleothem growth
E	Breakdown	Large and angular boulders broke off from the ceiling and walls of the cave

4.4.9 Facies D

Speleothems are chemical precipitation deposits formed inside caves. The Gran Dolina site has well-developed carbonate speleothems in TD1.1.1 and TD2.1 layers and minor growths in TD1.1.4, TD1.1.6, and TD1.1.8. The TD1.1.1 and TD2.1 speleothems are 50 cm thick lenticular-shaped layers and are well crystallized, showing several crystallization phases.

4.4.10 Facies E

Breakdown facies are characterized by large and angular boulders breaking off caves' ceiling and walls. This facies appears in the TD2.3 layer, where boulders larger than 50 cm are observed (Fig. 6E). The rock falls have caused sediment deformation in the underlying layers, as in the TD1.1 sub-unit, where laminated layers are folded because of the TD2.3 breakdown.

4.5 Soft-sediment deformation structures

The soft-sediment deformation structures are defined as "deformations that occur in still unlithified sediments or in sedimentary rocks that had not yet undergone lithification before the deformation structures started to be formed." (Van Loon, 2009). In TD1 and TD2, two kinds of soft-sediment deformation have been described (Campaña et al., 2015). On the one hand, the layers of the section show different dips (Fig. 4) through the south-west, TD1.2 layers have a dip of 30°, TD1.1 layers have a dip of 12°, that to the south-west increased to 33°, and finally TD2 are sub-horizontal with a dip of 15° to the south-west (Campaña et al., 2015). On the other hand, the breakdown of TD2.3 caused the folding of the underlying layers as TD1.1.2 and TD1.1.3. This deformation is formed by rounded, low-amplitude anticlines and synclines that conform to the shape of the breakdown.

5 Discussion

5.1 Comparison with previous works

In Campaña et al. (2017), seven autochthonous facies were differentiated in Gran Dolina (Table 1). Five were described
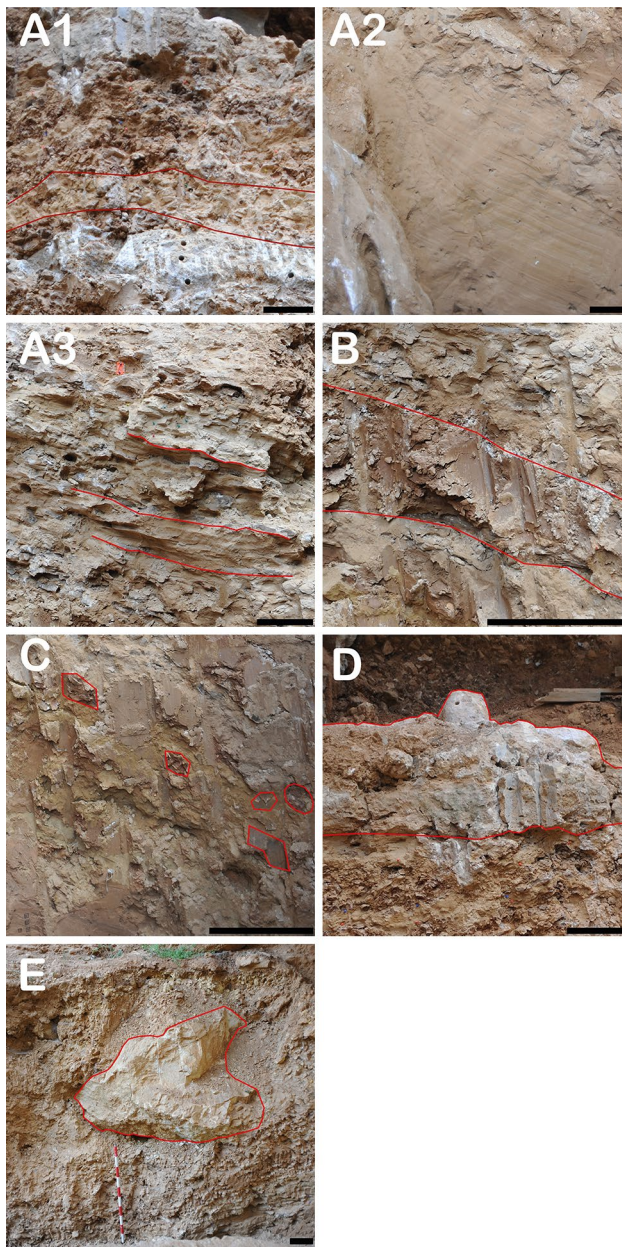
Fig. 6 Sedimentary facies of TD1 and TD2 sequence. **A1** Facies A1 of TD2.2 marked by red lines. **A2** Facies A2 of TD1.2.2. **A3** Facies A3 of TD1.1.3. Red lines indicate cemented layers. **B** Facies B of TD1.1.4 marked by red lines. **C** Facies C1 of TD1.1.7. Red lines mark the rip-up clasts. **D** Facies D of TD2.1. **E** Facies E of TD2.3. A red line marks the boulder. The black bar represents 25 cm

in TD1 and TD2 units: speleothem, breakdown, fluvial facies A, fluvial facies B and fluvial facies C. In the current work, the re-study of the nine meters of the current section has allowed us to reevaluate these facies and present a better classification. Speleothem and breakdown facies remain as defined, but the fluvial facies of Campaña et al. (2017) are discussed below.

Autochthonous fluvial facies were defined by Campaña et al. (2017) as "sediments deposited by the action of a more or less constant stream of groundwater that selects and concentrates particles of similar size. It is formed by well-sorted sands, which display a unimodal particle size distribution and usually include a very high percentage of quartz grains". These fluvial facies were differentiated into three sub-facies: facies A (FLA) as laminated sandy silt with soft nodules, facies B (FLB) as laminated clayey silt with cemented layers, and facies C (FLC) as sands and clays. The facies include in the current work include these facies. Thus, FLA is separated in facies A1 and facies A2, according to their particle size. FLB is the same that facies A3 since they have the same textural and fabric description. Finally, FLC includes sands and clays that in the current work have been separated in two different facies: sands are included in facies A1, while clays have been distinguished as facies B, defined as millimetric laminated clayed silt after particle size analysis.

5.2 Interpretation of the facies and depositional environments of TD1 and TD2

Facies A, defined as millimetric laminated yellowish brown sand and silt with rip-up clasts of silt and clay, shows similar features to other cave facies described in the bibliography, such as the channel facies described in the Mammoth Cave by Bosch and White (2004), facies Sh in Lapa Doce cave system (Laureano et al., 2016) or facies Laminated Sand in the caves of the Cheat River (Springer & Kite, 1997a, 1997b). These facies are composed of sand and silty sands with horizontal lamination and are interpreted as the result of a fluvial flow. The rip-up clasts indicate some energy in the hydric flow that was capable of eroding previous sedimentary deposits since these rip-up clasts are formed by silt and clay, and the energy needed to erode these cohesive sediments is similar to the required to erode and transport gravels (Herman et al., 2012; Sundborg, 1956). The lack of gravels in the deposit can be due to the lack of them in the source area or that the fissures were too small to allow the entry of them. This facies has three sub-facies. The facies A1 and A2 are very similar, differing only in that the main particle size component in facies A1 is sand, meanwhile in facies A2 is silt. This suggests that facies A2 represents a period with less energy than facies A1. Facies A3 shows cemented layers intercalated between the silty sand layers. These cemented layers, with some speleothem growth, indicate cycling cease of the hydric flow. Although some of these cemented layers can be post-depositional, the speleothem growths, that only appears in sub-aerial conditions, suggest that the drop of the water table caused the cementation. This major cycle contains other minor cycles that formed the lamination of the layers. Therefore, this facies

indicates a period with constant changes in the hydric flow, with cycling variations in the energy and numerous hiatuses.

Red mud facies are very common in caves (Bull, 1981; Springer & Kite, 1997a, 1997b; Auler et al., 2009; Martini, 2011; Iacoviello & Martini, 2012; Laureano et al.,; 2016; Martín-Perea et al., 2022). Facies B, defined as reddish brown millimetric laminated clay and silt, can be considered like these facies since it shows similar sedimentological features as lamination, color and particle size. These deposits have been explained as slackwater deposits that have been interpreted as the result of sequential flooding events that can build up very fine-scale layering (Bull, 1981; Herman et al., 2012), in some cases related to underground lakes (Martini, 2011).

The facies C1 do not show any internal structure or lamination, but the rip-up clasts observed in this facies indicates some energy in the flow and, therefore, some transport of the sediment. As in facies A, the rip-up clasts are formed by silt and clay that surely were eroded from older layers from inside the karst. The lack of sedimentary structures can indicate that this facies could be deposited in a single event.

As discussed above, facies similar to facies A, B, and C1 have been described by other authors as deposits from hydric flows associated with phreatic conditions (Bull, 1981; Springer & Kite, 1997a, 1997b; Lauretano et al., 2016; Kampolis et al., 2022). These facies are indicators of a more or less constant hydric regime inside the cave, which can be related to hydric processes at a regional level (Hunt et al., 2010; Wagner et al., 2011). This suggests that, at the time of the deposition of these facies, Gran Dolina was partially flooded below the water table (Springer & Kite, 1997a, 1997b). In this sense, facies A, B, and C1 would be considered as phreatic facies.

On the other side, the features of facies C2, a wall-supported massive silty sand deposit, suggest that its sedimentation could be related to runoff water from the cave wall that gradually accumulates it by accretion. It can be similar to backswamp facies described by Bosch and White (2004) that consists of "weathering residue of the bedrock and infiltrate material filtering into the conduit system from overlying soils with little or no lateral transport" (Bosch & White, 2004) and the FO facies in La Cala cave and Oscurusciuto rock shelter described as sandy silt without sedimentary structure that was deposited due to infiltration processes from overlying soils and sediments (Martini et al., 2018, 2021). In this case, the small amount of sand in the residue of the bedrock (Aleixandre & Pérez-González, 1999) indicates that this deposit is the result of the soil washdown, and, therefore, a slow sedimentation rate would be expected. In addition, the dip and geometry of the layer, with a wedge shape, could suggest that there was not any water table at the moment of the sedimentation.

The formation of speleothems (facies D) implies sub-aerial conditions, being an indicator of vadose conditions (Springer & Kite, 1997a, 1997b). During the growth of a speleothem, other sedimentary deposits should not occur; it means that a speleothem indicates a hiatus in the stratigraphic section (Gillieson, 1986). The speleothems of the section of TD1 and TD2 are found near the East wall. Vertically, they are located in the same line, suggesting a drip point in this site that was active during most TD1 and TD2 sedimentation.

Breakdown deposits (facies E) are very common deposits in caves (e.g. Gillieson, 1996; Martini et al., 2018; White, 2007). Causes of collapse can be because of undermining of the underlying support, loss of hydrostatic pressure caused by the transition from phreatic to vadose conditions, cryoclastism, secondary mineral wedging, or earthquakes (Sasowsky, 2007). The deformation of the underlying layers in TD1 suggests the fall of the rocks from a high height, perhaps the ceiling of the cave.

According to the previously described features of the sedimentary facies, it can be considered that TD1 and TD2 represent a period of repetitive variations in the water table level, with fluctuations between phreatic conditions, indicated by the deposits of facies A, B, and C1; and vadose conditions, indicated by cementation and facies C2, D and E. These fluctuations can indicate that Gran Dolina was in the epiphreatic zone, but on the one hand, the formation of speleothem needs stable vadose conditions during long time (Ford & Williams, 2007), and in the other hand, the continuous lamination of facies A and facies B in sub-units with more than one meter of thick suggests stable phreatic conditions (Gillieson, 1996; Springer & Kite, 1997a, 1997b). Therefore, the epiphreatic conditions have been used only in deposits where the changes in the conditions were clearly fast, as putatively in the facies A3 (Fig. 3), being not possible to differentiate precisely the phreatic and vadose conditions.

These deposits can generally be considered as the result of an underground fluvial flow that transports sediments from farther sources than entrance facies. Furthermore, the fact that in certain cementations, a speleothem develops, as in layers TD1.1.6 and TD1.1.8, suggests that the cementations were produced by sedimentary stops and aerial exposure. Therefore, the cementations found in the TD1 and TD2 sequence would indicate vadose conditions (Springer & Kite, 1997a, 1997b). Based on the last dating study of TD1, which inferred an age of about 1.4 Ma for the base of this deposit (Duval et al., 2022), the sedimentation of Gran Dolina cave began shortly after its vadose incision. TD1.2 represents the first registered sedimentation of Gran Dolina cave; it starts with the layer TD1.2.4 composed of laminated silty sand (facies A1) dipping towards the West. At the top of this layer, the lamination

Fig. 7 Summary stratigraphic column, with all layers of TD1 and TD2 (same legend as Fig. 3). Magnetostratigraphic succession (Duval et al., 2022; Parés et al., 2018)—P: Punaruu, CM: Cobb Mountain. Environment—Blue: phreatic conditions. Greyish blue: quick alternating of phreatic and vadose conditions. Red: vadose conditions. Discontinuities and energy flow—Solid bold line: major discontinuity. Solid fine line: medium discontinuity. Discontinuous line: small discontinuity. L: Low energy. M: Medium energy. H: High energy
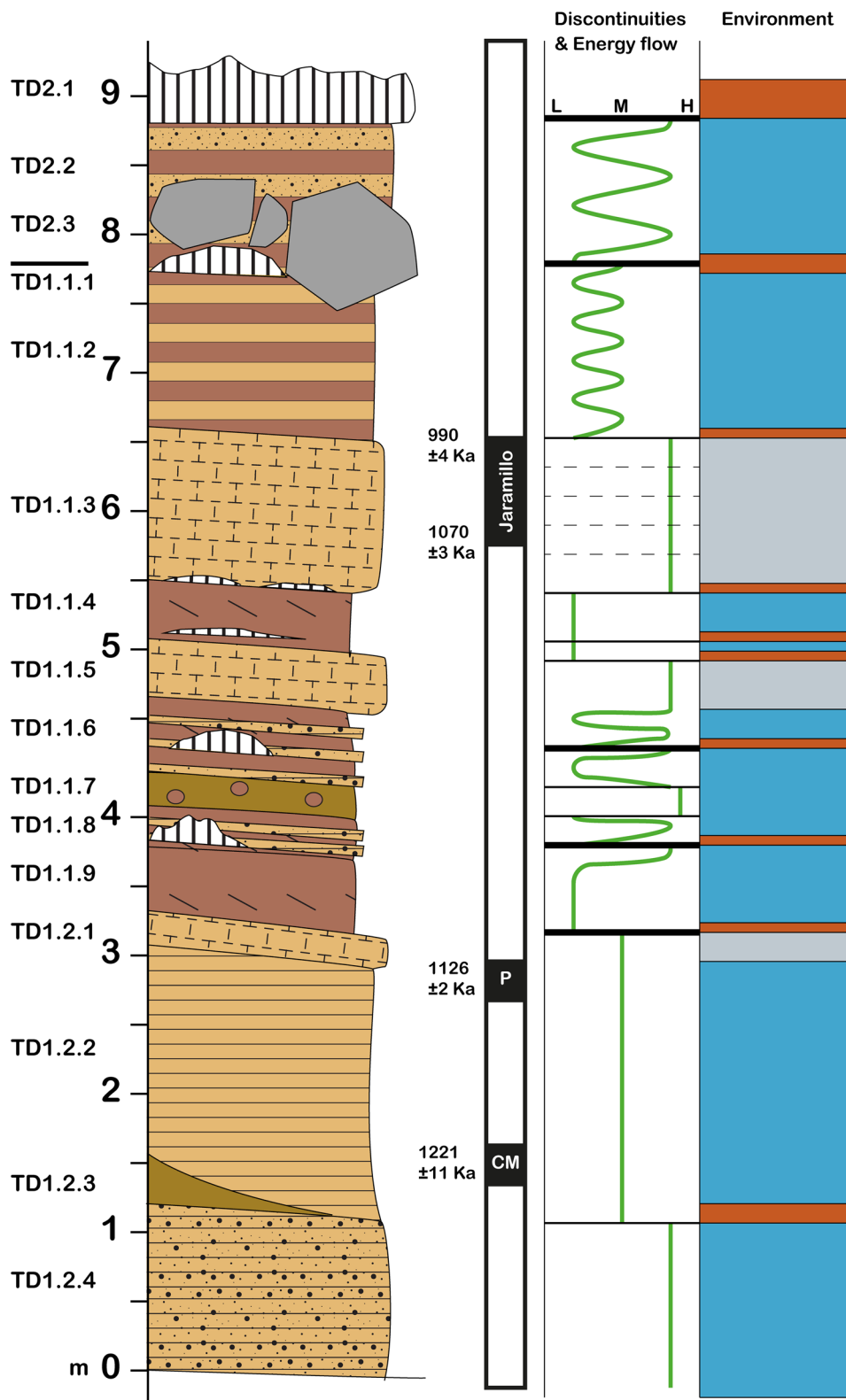
is truncated by an erosive surface, above which TD1.2.3 is deposited. This layer is accretion sediment that, with the erosive surface, suggests a stop in the phreatic sedimentation in the sequence that would indicate the first registered vadose conditions in Gran Dolina cave after the vadose incision of the cave (Fig. 7). The sedimentation is reactivated with laminated sandy silt (facies A2) of TD1.2.2 which suggests the return of phreatic conditions in the

cave, but with lesser energy than in TD1.2.4. Finally, at the top of TD1.2, the cementation of TD1.2.1 would indicate vadose conditions and another hiatus in the sequence.

The TD1.1 sub-unit shows an important change in the dynamic of the sedimentation. From now on, the sedimentation is dominated by centimeter-thick or decimeter-thick cycles of laminated silty sand, in some cases cemented (facies A1 and A3); and laminated clayed silt (facies B), within each of which a millimetric cyclical lamination can be observed (Figs. 4 and 7). In addition, there are at least four speleothems and a level of facies C1. All these levels indicate a moment with successive hydric changes from decreased energy when the clays of facies B are deposited; to increased energy, when the silts of facies A are deposited. The end of some cycles with speleothem would indicate the drop of the water table and vadose conditions (Springer & Kite, 1997a, 1997b). It is especially remarkable in TD1.1.4 where two layers of speleothem are observed (Fig. 4). The layer TD1.1.7, massive silty sands with rip-up clasts (facies C1), indicates a break in these cycles, with the reworking of previous deposits of the cave. This can be due to local changes inside the karst system, such as variations in the course of the water flow and reworking of near deposits.

These cycles thicken towards the top until TD1.1.4 and TD1.1.3, that has about 1.5 m thick. This increase in thickness may be related to temporal increases in the environmental cycles that regulate this sedimentation and more stable conditions than in the underlying cycles.

Furthermore, TD1.1.2 shows an alternating of facies A2 and facies B that suggests a relative water table rise and stable phreatic conditions in Gran Dolina cave, although with a difference in the energy flow. This layer presents partial cementation, but as they are only observed in facies B, namely, in clayey silt layers, and no speleothem growths are observed in these layers, it is preliminary interpreted as by post-depositional cementation of the most clayey layers. Finally, the water level falls again, allowing the speleothem growth at the top (TD1.1.1).

The TD2 unit starts with a breakdown (facies E) of more than 1-m diameter boulders that caused deformation in the layers of TD1.1 (Fig. 6E). These boulders collapsed from the walls and the ceiling of the cave. Later, TD2.2 is deposited with a similar pattern to TD1.1.2, an alternating of facies A1 and facies B. This indicates the last phreatic condition in the cave (Fig. 7), with substantial energy flow fluctuations. The particle size of facies A1 suggests more energy in TD2.2 than in TD1.1.2. Finally, the TD2 unit ends sealed by more than 40 cm thick speleothem which indicates a relatively long time before the entry of the entrance facies of TD3 and TD4 (Campaña et al., 2017). The variations of the TD1 and TD2 sediments indicate that, in a broad temporal sense, Gran Dolina would be in the epiphreatic zone of the hydric regime, with the base level oscillating about the altitude of

the cavity, but never completely flooding it. These oscillations would reflect the changes in the hydrogeological basin of the Arlanzón River since karst systems are more sensitive to changes in the water table: oscillations of centimeters outside can imply metric rises or falls inside karst (Ford & Williams, 2007). These variations should be related to the transition between the terraces T3 and T4, which is related to the vadose incision in Gran Dolina cave (Benito-Calvo et al., 2017). The variations between vadose and phreatic conditions observed in the TD1 and TD2 stratigraphic sequence suggest that this transition had, at least, ten stages (Fig. 7). The TD2.1 speleothem would mark the final phreatic influence and deposition of interior facies in Gran Dolina cave related to the T3-T4 transition, which would finish with the final construction of the terrace T4 in the hydrogeological basin of the Arlanzón River. This terrace has an estimated age of about 0.85 Ma (Benito-Calvo et al., 2017; Moreno et al., 2012) which is consistent with the proposed dates for the end of TD2 (about 0. 89 Ma; Duval et al., 2022). This stratigraphic section mainly matches with the Railway Trench borehole (BH2 in Bermejo et al., 2020), composed of fine clays and fine sands. The limitation of the mechanical drilling is that it avoids observing the sedimentary details in the borehole and prevents a direct correlation between it and the main section. Nonetheless, this borehole and the GPR survey demonstrate that Gran Dolina cave continues to the west (Bermejo et al., 2020), and, therefore, the flow direction was from east to west.

5.3 Sedimentation rate and paleoclimate

TD1 and TD2 units are proposed to develop during about 400 kyr, according to TT-OSL, ESR, and palaeomagnetic dating results (Duval et al., 2022). In TD1, three magnetic excursions have been described, tentatively identified as Cobb Mountain (1221 ± 11 ka, Channel et al., 2020), Punaruu (1126 ± 2 ka, Channel et al., 2020), and Jaramillo (from 1070 ± 3 ka to 990 ± 4 ka, Channel et al., 2020) from bottom to top. Cobb Mountain and Punaruu are found near the bottom and the top of the TD1.2.2 layer, respectively (Fig. 7) (Duval et al., 2022). This is a 1.8 m level that shows no apparent sedimentary discontinuity (Table 2). Therefore, an approximate sedimentation rate of 1.89 cm/kyr can be calculated for this layer. If we assume that this sedimentation rate was constant from TD1.2.2 to the bottom of the sequence, an age of 1.31 Ma can be tentatively proposed for the beginning of the sequence, which agrees with the numerical TT-OSL age estimate of 1.30 ± 0.14 Ma presented by Duval et al. (2022), near to the bottom of the infill, but is younger than the 1.44 Ma estimated by these authors. In the first instance, one may note that the existing climate oscillations between Cobb Mountain and Punaruu magnetic events

are apparently not registered in this sedimentary record, although future studies specifically focused on the millimetric laminations of this layer could find them.

Between the magnetic excursion Punaruu and the base of Jaramillo 56 kyr passed, and there is about a 3 m thick TD1 sequence that corresponds from TD1.2.1 to the middle of TD1.1.3. Then, an approximate sedimentation rate of 5.35 cm/kyr can be calculated for these layers. This sedimentation rate is significantly higher than that calculated for TD1.2.2, even more so if we take into consideration that TD1.2 is a more continuous record than TD1.1, where some hiatuses are identified (Fig. 7). If the magnetic excursion Punaruu is not considerate and the sedimentation rate is calculated from Cobb Mountain, an approximate sedimentation rate of 3.04 cm/kyr is obtained. If these estimations are correct, it would mean that sedimentation rates in TD1 would be inconsistent between layers, and that age estimation by sedimentation rate must be viewed with caution. The time between Punaruu and the base of Jaramillo is related to the Marine Isotope Stage 32. Then, the changes observed in TD1.1 cannot associate with the Marine Isotope Stages. The alternation of facies B and facies A of TD1.1 may be due to thousand-year environmental cycles.

5.4 Soft-sediment deformation structure of the stratigraphic sequence

The soft-sediment deformation structure inside a cave, where tectonics is not contemplated, can be assigned to post-depositional processes such as the collapse of the cave floor, erosion of the lower levels, or loss of volume of the underlying sediments due to desiccation or compaction (Marean et al., 2004; Van Loon, 2009).

The eastern section, close to the cave wall, does not show this deformation. This may be due to the successive speleothems and cementations found in this area of the section, could suggest that the compaction of the sediments formed the deformation due to the weight of the upper lithostratigraphic units or that undermining processes of lower layers occurred to the west. This eastern area could preserve undeformed by two factors: on the one hand, the speleothems served as support and, on the other hand, the absence of large masses of sediment vertically in the eastern area, since part of the cave wall closes in that zone avoiding the sedimentary accumulation of entrance facies on it (Campaña et al., 2017).

5.5 Source of the sediment ¿Autochthonous sediments?

The autochthonous facies have been defined as the materials that are derived locally within the cave (White, 2007). Different sediments have been included in autochthonous facies, such as weathering detritus, speleothem, breakdown, infiltrates, or guano (Goldberg & Sherwood, 2006; White, 2007). One of the possible origins that have been postulated for the sediments found inside the karst of the Sierra de Atapuerca, as TD1 and TD2 units, is the weathering detritus (Campaña et al., 2017; Ortega et al., 2013; Pérez-González et al., 1999). It is the sediment derived from insoluble residues in the bedrock and is found as sand, silt, and clay deposits with evidence of little or no stream transport. As the process for accumulating this type of sediment is relatively slow, it is usually deposited in areas without other types of sedimentation, i.e., in isolated areas or far from inputs of sediments from outside. For this reason, it usually appears inside the endokarst or at the base of the sedimentary cave infills, where this sediment is deposited before the cave's opening to the outside. Although we cannot ignore a certain influence of this residue on the sediment, the low percentage of residue in the Sierra de Atapuerca limestone, less than 0.1 g per kg (Aleixandre & Pérez-González, 1999), suggests that there is another source for the nine meters of sedimentary fill found at the base of Gran Dolina.

Therefore, of the five main facies observed in TD1 and TD2, only facies D (Speleothem) and facies E (Breakdown) can be included in this definition of autochthonous facies, since Facies A, B, and C shows characteristics that indicate a certain transport, as discussed above, such as the horizontal lamination, the predominance of quartz in the mineralogy, the presence of rip-up clasts and the particle size dominate of sand in some layers.

The mineralogy of the sediments is very similar in all the stratigraphic section (Table 4), indicating that the source of the sediments is the same, and, therefore, that the changes in the granulometry are due to changes in the hydric regime. The richness of sand particle size observed in some layers in TD1 and TD2 (Fig. 5), e.g. TD2.2 or TD1.1.5, contrasts with the little sand found in the residue of the Sierra de Atapuerca limestone (Aleixandre & Pérez-González, 1999). In addition, the ESR and TT-OSL dates suggest the lack of heritage sand from the limestone (Duval et al., 2022). This evidence suggests a source of the sediment outside of the karstic system, being the sediment added by a fluvial stream that selected the sediment and entry into the karstic system from a relatively far entrance. The location of this entry is unknown since the intermediate level of the karst is not entirely known, although the southern contact between the Sierra de Atapuerca and the valley of the Arlanzón River has been postulated as a possible entry of these sediments (Ortega & Martín-Merino, 2019).

Therefore, the suitability of the term 'autochthonous' to describe TD1 and TD2 facies should be reconsidered.

Springer and Kite (1997a, 1997b) separated the cave sediments into three categories: phreatic, vadose, and residual. As mentioned before, facies A, B, and C can be included in the phreatic category, but facies D and E are vadose facies since speleothems and gravity falls are formed in vadose conditions.

Other authors have used interior facies to define this kind of sediments (Kukla & Lozek, 1958; Creer & Kopper, 1976; Sroubek et al., 2007). This terminology refers to the distance at which an entry is located; thus, the interior facies is defined as the sediments found deeper in the cave, beyond the reach of surface weathering. In this environment, clays, silts, and sands predominate and are described as accumulation by fluvial flows (Creer & Kopper, 1976; Springer & Kite, 1997a, 1997b; Bosch & White, 2004; Sroubek et al., 2007). Since the sedimentological study suggests that facies A, B, and C can be interpreted as transported sediment by fluvial flows, in agreement with particle shape analyses (Campaña et al., 2016), the use of interior facies (and entrance facies for allochthonous facies), seems to be more suitable to the conditions observed in Gran Dolina than the previous classification of Allochthonous and Autochthonous (Campaña et al., 2017) (Table 1).

6 Conclusion

TD1 and TD2 units are 9 m thick of interior facies in the base of Gran Dolina cave. This sedimentation began shortly after its vadose incision in the Early Pleistocene and was directed by the fluctuations in the level of the water table that caused the succession of phreatic and vadose phases, which would indicate general epiphreatic conditions inside the cave. Flooding processes deposited millimetric laminated sand and silts during phreatic conditions, while during vadose conditions, speleothem growths and cementations occurred.

These deposits have been defined as interior facies since they were deposits the inside of the cave when there was no entrance nearby. This terminology replaces the previous autochthonous term because it is more exact with the features observed in TD1 and TD2 units. The interior facies are divided by hydrological conditions. The phreatic facies (A, B, and C1) resulted from an underground fluvial flow that transported sediments from the outside to the inside of the cave. These sediments entered the cave from an entry situated in the contact between the Sierra de Atapuerca and the Arlanzon valley. The vadose facies (C2, D, and E) were deposited when the water table was below the sedimentation level, and they were formed by accretion, dripping, or falls.

At least ten stages of phreatic-vadose conditions have been identified, but indeed there are more. These stages should be related to the evolution of Arlanzón catchment during the transition between terrace T3 and terrace T4.

The sedimentation rate calculated by available geochronological data suggest great variation in sedimentation. The bottom of the sequence (from unit TD1.2.2 to TD1.2.4) has a sedimentation rate of 1.89 cm/kyr, while the TD1.1 deposits have an approximate sedimentation rate of 5.35 cm/kyr.

References

Aleixandre, T., & Pérez-González, A. (1999). Facies mineralógicas de las arenas de los rellenos kársticos de la Sierra de Atapuerca (Burgos). In B. Andreo, F. Carrasco, & J. J. Durán (Eds.), *Contribución del estudio científico de las cavidades kársticas al conocimiento geológico* (pp. 231–242).

Angelucci, D. E., & Zilhão, J. (2009). Stratigraphy and formation processes of the upper pleistocene deposit at Gruta da Oliveira, almonda karstic system, Torres Novas. *Portugal. Geoarchaeology, 24*(3), 277–310. https://doi.org/10.1002/gea.20267

Arriolabengoa, M., Iriarte, E., Aranburu, A., Yusta, I., & Arrizabalaga, A. (2015). Provenance study of endokarst fine sediments through mineralogical and geochemical data (Lezetxiki II cave, northern Iberia). *Quaternary International, 364*, 231–243. https://doi.org/10.1016/j.quaint.2014.09.072

Auler, A. S., Smart, P. L., Wang, X., Piló, L. B., Edwards, R. L., & Cheng, H. (2009). Cyclic sedimentation in Brazilian caves: Mechanisms and palaeoenvironment significance. *Geomorphology, 106*, 142–153.

Benito-Calvo, A., Pérez-González, A., & Parés, J. M. (2008). Quantitative reconstruction of Late Cenozoic landscapes: A case study in

the Sierra de Atapuerca (Burgos, Spain). *Earth Surface Processes and Landforms, 33*(2), 196–208.

Benito-Calvo, A., & Pérez-González, A. (2015). Geomorphology of the Sierra de Atapuerca and the Middle Arlanzón Valley (Burgos, Spain). *Journal of Maps, 11*(4), 535–544. https://doi.org/10.1080/17445647.2014.909339

Benito-Calvo, A., Ortega, A. I., Pérez-González, A., Campaña, I., Bermúdez de Castro, J. M., & Carbonell, E. (2017). Palaeogeographical reconstruction of the Sierra de Atapuerca Pleistocene sites (Burgos, Spain). *Quaternary International, 433*, 379–392. https://doi.org/10.1016/j.quaint.2015.10.034

Benito-Calvo, A., Ortega, A. I., Navazo, M., Moreno, D., Pérez-Gonzalez, A., Parés, J. M., Bermúdez De Castro, J. M., & Carbonell, E. (2018). Pleistocene geodynamic evolution of the Arlanzón valley: Implications for the formation of the endokarst system and the open air archaeological sites of the Sierra de Atapuerca (Burgos, España). *Boletín Geológico y Minero, 129*, 059–082.

Berger, G. W., Pérez-González, A., Carbonell, E., Arsuaga, J. L., Bermúdez de Castro, J. M., & Ku, T. L. (2008). Luminescence chronology of cave sediments at the Atapuerca paleoanthropological site. *Spain. Journal of Human Evolution, 55*(2), 300–311.

Bermejo, L., Ortega, A. I., Guérin, R., Benito-Calvo, A., Pérez-González, A., Parés, J. M., Aracil, E., Bermúdez de Castro, J. M., & Carbonell, E. (2017). 2D and 3D ERT imaging for identifying karst morphologies in the archaeological sites of Gran Dolina and Galería Complex (Sierra de Atapuerca, Burgos, Spain). *Quaternary International, 433*, 393–401.

Bermejo, L., Ortega, A. I., Parés, J. M., Campaña, I., Bermúdez de Castro, J. M., Carbonell, E., & Conyers, L. B. (2020). Karst features interpretation using ground-penetrating radar: A study from the Sierra de Atapuerca, Spain. *Geomorphology, 367*, 1–14.

Bermejo, L. (2021). Reconocimiento de morfologías endokársticas y yacimientos en los karst de la Sierra de Atapuerca y Ojo Guareña (Burgos) mediante técnicas de prospección geofísica. *Ph.D Thesis.* University of Burgos, Spain.

Blott, S. J., & Pye, K. (2012). Particle size scales and classification of sediment types based on particle size distributions: Review and recommended procedures. *Sedimentology, 59*(7), 2071–2096.

Bonifay, E. (1956). Les sédiment détritiques grossiers dans les remplissages des grottes. *L'anthropologie, 5–6*, 447–461.

Bosch, R., & White, W. B. (2004). Lithofacies and transport of clastic sediments in karstic aquifers. In I. D. Sasowsky, J. Mylroie, R. Bosch, & W. B. White (Eds.), *Studies of Cave Sediments* (pp. 1–22). Springer.

Bull, P. A. (1981). Some fine-grained sedimentation phenomena in caves. *Earth Surface Processes & Landforms, 6*(1), 11–22.

Campaña, I., Benito-Calvo, A., Pérez-González, A., Ortega, A. I., de Castro, B. J. M., & Carbonell, E. (2015). Using 3D models to analyse stratigraphic and sedimentological contexts in archaeo-palaeo-anthropological pleistocene sites (Gran Dolina Site, Sierra De Atapuerca). In CAA2015. Keep The Revolution Going: Proceedings of the 43rd Annual Conference on Computer Applications and Quantitative Methods in Archaeology (pp. 337–345). https://www.scopus.com/inward/record.uri?eid=2-s2.0-85091076214&partnerID=40&md5=b82f17d4b47c42a2588e1ec56cb3d25b.

Campaña, I., Benito-Calvo, A., Pérez-González, A., Bermúdez de Castro, J. M., & Carbonell, E. (2016). Assessing automated image analysis of sand grain shape to identify sedimentary facies, Gran Dolina archaeological site (Burgos, Spain). *Sedimentary Geology, 346*, 72–83. https://doi.org/10.1016/j.sedgeo.2016.09.010

Campaña, I., Benito-Calvo, A., Pérez-González, A., Ortega, A. I., Bermúdez de Castro, J. M., & Carbonell, E. (2017). Pleistocene sedimentary facies of the Gran Dolina archaeo-paleoanthropological site (Sierra de Atapuerca, Burgos, Spain). *Quaternary International, 433*, 68–84. https://doi.org/10.1016/j.quaint.2015.04.023

Campaña, I. (2018). Estratigrafía y sedimentología del yacimiento de Gran Dolina (Sierra de Atapuerca, Burgos). *Ph.D Thesis.* University of Burgos, Spain.

Carbonell, E., García-Antón, M. D., Mallol, C., Mosquera, M., Ollé, A., Rodríguez, X. P., Sahnouni, M., Sala, R., & Vergès, J. M. (1999). The TD6 level lithic industry from Gran Dolina, Atapuerca (Burgos, Spain): Production and use. *Journal of Human Evolution, 37*(3–4), 653–693. https://doi.org/10.1006/jhev.1999.0336

Carbonell, E., Bermúdez De Castro, J. M., Parés, J. M., Pérez-González, A., Cuenca-Bescós, G., Ollé, A., Mosquera, M., Huguet, R., Van Der Made, J., Rosas, A., Sala, R., Vallverdú, J., García, N., Granger, D. E., Martinón-Torres, M., Rodríguez, X. P., Stock, G. M., Vergès, J. M., Allué, E., & Arsuaga, J. L. (2008). The first hominin of Europe. *Nature, 452*(7186), 465–469.

Channel, J. E. T., Singer, B. S., & Jicha, B. R. (2020). Timing of Quaternary geomagnetic reversals and excursions in volcanic and sedimentary archives. *Quaternary Science Reviews, 228*, 106114.

Chung, F. H. (1975). Quantitative interpretation of X-Ray diffraction patterns. III. Simultaneous determination of a set of reference intensities. *Journal of Applied Crystallography, 8–1*, 17–19.

Cooke, H. B. S. (1938). The Sterkfontein bone breccia: A geological note. *South African Journal of Science, 35*, 204–208.

Creer, K. M., & Kopper, J. S. (1976). Secular oscillations of the geomagnetic field recorded by sediments deposited in caves in the mediterranean region. *Geophysical Journal International, 45*(1), 35–58. https://doi.org/10.1111/j.1365-246X.1976.tb00312.x

Demuro, M., Arnold, L. J., Parés, J. M., Pérez-González, A., Ortega, A. I., Arsuaga, J. L., Bermúdez de Castro, J. M., & Carbonell, E. (2014). New luminescence ages for the Galería Complex archaeological site: Resolving chronological uncertainties on the Acheulean record of the Sierra de Atapuerca, Northern Spain. *PLoS ONE, 9* (10).

Duval, M., Arnold, L. J., Demuro, M., Parés, J. M., Campaña, I., Carbonell, E., & Bermúdez de Castro, J. M. (2022). *New chronological constraints for the lowermost stratigraphic unit of Atapuerca Gran Dolina (Burgos, N Spain).* In press.

Duval, M., Grün, R., Parés, J. M., Martín-Francés, L., Campaña, I., Rosell, J., Shao, Q., Arsuaga, J. L., Carbonell, E., & Bermúdez de Castro, J. M. (2018). The first direct ESR dating of a hominin tooth from Atapuerca Gran Dolina TD-6 (Spain) supports the antiquity of *Homo antecessor*. *Quaternary Geochronology, 47*, 120–137.

Falguères, C., Bahain, J.-J., Bischoff, J. L., Pérez-González, A., Ortega, A. I., Ollé, A., Quiles, A., Ghaleb, B., Moreno, D., Dolo, J.-M., Shao, Q., Vallverdú, J., Carbonell, E., Bermúdez de Castro, J. M., & Arsuaga, J. L. (2013). Combined ESR/U-series chronology of Acheulian hominid-bearing layers at Trinchera Galería site, Atapuerca, Spain. *Journal of Human Evolution, 65*, 168–184.

Falguères, C., Bahain, J. J., Yokoyama, Y., Arsuaga, J. L., Bermudez De Castro, J. M., Carbonell, E., Bischoff, J. L., & Dolo, J. M. (1999). Earliest humans in Europe: The age of TD6 Gran Dolina, Atapuerca Spain. *Journal of Human Evolution, 37*(3–4), 343–352.

Farrand, W. R. (2001). Sediments and stratigraphy in rockshelters and caves: A personal perspective on principles and pragmatics. *Geoarchaeology - an International Journal, 16*(5), 537–557.

Farrant, A. R., & Smart, P. L. (2011). Role of sediment in speleogenesis; sedimentation and paragenesis. *Geomorphology, 134*(1–2), 79–93.

Ford, D. C., & Williams, P. (2007). Karst Hydrogeology and Geomorphology. John Wily & Son, Ltd.

Fornós, J. J., Ginés, J., & Grácia, F. (2009). Present-day sedimentary facies in the coastal karst caves of Mallorca Island (western mediterranean). *Journal of Cave and Karst Studies, 71*(1), 86–99.

Gil, E., Aguirre, E., & Hoyos, M. (1987). Contexto Estratigráfico. In E. Aguirre, E. Carbonell, & J. M. Bermúdez de Castro (Eds.), El

hombre fósil de Ibeas y el Pleistoceno de la Sierra de Atapuerca. Junta de Castilla y León.

Gillieson, D. (1986). Cave sedimentation in the New Guinea highlands. *Earth Surface Processes and Landforms, 11*, 533–543.

Gillieson, D. (1996). *Caves: Processes, Development and Management*. Ed. Blackwell Publishers.

Goldberg, P., & Sherwood, S. C. (2006). Deciphering human prehistory through the geoarchaeological study of cave sediments. *Evolutionary Anthropology, 15*, 20–36.

Gómez-Olivencia, A., Carretero, J. M., Lorenzo, C., Arsuaga, J. L., Bermúdez de Castro, J. M., & Carbonell, E. (2012). The costal skeleton of Homo antecessor: Preliminary results. *Journal of Human Evolution, 59*(6), 620–640. https://doi.org/10.1016/j.jhevol.2010.07.023

Herman, E. K., Toran, L., & White, W. B. (2012). Clastic sediment transport and storage in fluviokarst aquifers: An essential component of karst hydrogeology. *Carbonate Evaporites, 27*, 211–241.

Huguet, R., Vallverdú, J., Rodríguez-Álvarez, X. P., Terradillos-Bernal, M., Bargalló, A., Lombera-Hermida, A., Menéndez, L., Modesto-Mata, M., Van der Made, J., Soto, M., Blain, H.-A., García, N., Cuenca-Bescós, G., Gómez-Merino, G., Pérez-Martínez, R., Expósito, I., Allué, E., Rofes, J., Burjachs, F., … Carbonell, E. (2017). Level TE9c of Sima del Elefante (Sierra de Atapuerca, Spain): A comprehensive approach. *Quaternary International, 433*, 278–295.

Hunt, C., Davison, J., Inglis, R., Farr, L., Reynolds, T., & Simpson, D. (2010). Site formation processes in caves: The Holocene sediments of the Haua Fteah, Cyrenaica. *Libya. Journal of Archaeological Science, 37*(7), 1600–1611.

Iacovello, F., & Martini, I. (2012). Provenance and geological significance of red mud and other clastic sediments of the Mugnano Cave (Montagnola Senese, Italy). *International Journal of Speleology, 41*(2), 317–328.

Kadlec, J., Chadima, M., Lisá, L., Hercman, H., Osintsev, A., & Oberhänsli, H. (2008). Clastic cave deposits in botovskaya cave (Eastern Siberia, Russian federation). *Journal of Cave and Karst Studies, 70*(3), 142–155.

Kampolis, I., Triantafyllidis, S., Skliros, V., & Kamperis, E. (2022). Quaternary evolutionary stages of Selinitsa Cave (SW Peloponnese, Greece) reveal sea-level changes based on 3D scanning, geomorphological, biological, and sedimentological indicators. *Quaternary, 5*, 24. https://doi.org/10.3390/quat5020024

Kukla, J., & Lozek, V. (1958). K. problematica vyzkumu jeskynnich vyplni (Concerning the problems of the investigation of cave sediments). *Ceskoslov Kras, 2*, 19–83.

Laureano, F. V., Karmann, I., Granger, D. E., Auler, A. S., Almeida, R. P., Cruz, F. W., Strícks, N. M., & Novello, V. F. (2016). Two million years of river and cave aggradation in NE Brazil: Implications for speleogenesis and landscape evolution. *Geomorphology, 273*, 63–77.

Marean, C. W., Nilssen, P. J., Brown, K., Jerardino, A., & Stynder, D. (2004). Paleoanthropological investigations of Middle Stone Age sites at Pinnacle Point, Mossel Bay (South Africa): Archaeology and hominid remains from the 2000 Field Season. *PaleoAnthropology*.

Martín-Merino, M. A., Domingo, S., & Antón, T. (1981). Estudio de las cavidades de la zona BU-IV A (Sierra de Atapuerca). *Kaite, 2*, 41–76.

Martín-Perea, D. M., Maíllo-Fernández, J. M., Marín, J., Arroyo, X., & Asiaín, R. (2022). A step back to move forward: a geological re-evaluation of the El Castillo Cave Middle Palaeolithic lithostratigraphic units (Cantabria, northern Iberia). *Journal of Quaternary Science*, 1–14.

Martini, I. (2011). Cave clastic sediments and implications for speleogenesis: New insights from the Mugnano Cave (Montagnola

Senese, Northern Apennines, Italy). *Geomorphology, 134*(3–4), 452–460.

Martini, I., Ronchitelli, A., Arrighi, S., Capecchi, G., Ricci, S., Scaramucci, S., Spagnolo, V., Gambassini, P., & Moroni, A. (2018). Cave clastic sediments as a tool for refining the study of human occupation of prehistoric sites: Insights from the cave site of La Cala (Cilento, southern Italy). *Journal of Quaternary Science, 33*(5), 586–596.

Martini, I., Baucon, A., & Boschin, F. (2021). Depositional processes and environmental settings in rock shelters: The case of the prehistoric Oscurusciuto site (Southern Italy). *Geological Magazine, 158*, 891–904. https://doi.org/10.1017/S0016756820001041

Moreno, D., Falguères, C., Pérez-González, A., Duval, M., Voinchet, P., Benito-Calvo, A., Ortega, A. I., Bahain, J. J., Sala, R., Carbonell, E., Bermúdez de Castro, J. M., & Arsuaga, J. L. (2012). ESR chronology of alluvial deposits in the Arlanzón valley (Atapuerca, Spain): Contemporaneity with Atapuerca Gran Dolina site. *Quaternary Geochronology, 10*, 418–423. https://doi.org/10.1016/j.quageo.2012.04.018

Moreno, D., Falguères, C., Pérez-González, A., Voinchet, P., Ghaleb, B., Despriée, J., Bahain, J.-J., Sala, R., Carbonell, E., Bermúdez de Castro, J. M., & Arsuaga, J. L. (2015). New radiometric dates on the lowest stratigraphical section (TD1 to TD6) of Gran Dolina site (Atapuerca, Spain). *Quaternary Geochronology, 30*, 535–540.

Ollé, A., Mosquera, M., Rodríguez, X. P., de Lombera-Hermida, A., García-Antón, M. D., García-Medrano, P., Peña, L., Menéndez, L., Navazo, M., Terradillos, M., Bargalló, A., Márquez, B., Sala, R., & Carbonell, E. (2013). The Early and Middle Pleistocene technological record from Sierra de Atapuerca (Burgos, Spain). *Quaternary International, 295*, 138–167.

Ortega, A. I. (2009). *La Evolución Geomorfológica del karst de la Sierra de Atapuerca (Burgos) y su relación con los yacimientos pleistocenos que contiene*. Universidad de Burgos, Facultad de Humanidades y Educación.

Ortega, A. I., Benito-Calvo, A., Pérez-González, A., Martín, M. Á., Pérez, R., Parés, J. M., Aramburu, A., Arsuaga, J. L., Bermúdez de Castro, J. M., & Carbonell, E. (2013). Evolution of multilevel caves in the Sierra de Atapuerca (Burgos, Spain) and its relation to human occupation. *Geomorphology, 196*, 122–137.

Ortega, A.I., Benito-Calvo, A., Pérez-González, A., Carbonell, E., Bermúdez de Castro, J.M., Arsuaga, J.L. (2014). Atapuerca Karst and its Palaeoanthropological Sites, en F. Gutiérrez, M. Gutiérrez (eds.): Landscapes and Landforms of Spain, World Geomorphological Landscapes (pp. 101–110).

Ortega, A. I., Benito-Calvo, A., Martín, M. A., Pérez-González, A., Parés, J. M., Bermúdez de Castro, J. M., Arsuaga, J. L., & Carbonell, E. (2018). Las cuevas de la Sierra de Atapuerca y el uso humano del paisaje kárstico durante el Pleistoceno (Burgos, España). *Boletín Geológico y Minero, 129*(1/2), 83–105.

Ortega, A. I., & Martín-Merino, M. A. (2019). La terraza del sondeo de la Cantera Cudillo (La Paredeja) y su posible relación con la de Cueva del Silo, Cueva Peluda y Trinchera Elefante. *Cubía, 23*, 54–56.

Ossowski, G. (1882). Trzecie sprawozdanie z badan antropologiczno-archeologicznych w jaskiniach okolic Krakowa w 1881. *Zbiór Wiadomosci Do Atropologii Krajowej, 6*, 28–53.

Springer, G. S., & Kite, J. S. (1997a). River-derived slackwater sediments in caves along Cheat River, West Virginia. *Geomorphology, 18*, 91.

Šroubek, P., Diehl, J. F., & Kadlec, J. (2007). Historical climatic record from flood sediments deposited in the interior of Spirálka Cave, Czech republic. *Palaeogeography, Palaeoclimatology, Palaeoecology, 251*(3–4), 547–562.

Pablos, A., Lorenzo, C., Martínez, I., Bermúdez de Castro, J. M., Martinón-Torres, M., Carbonell, E., & Arsuaga, J. L. (2012). New foot remains from the Gran Dolina-TD6 Early Pleistocene site (Sierra

de Atapuerca, Burgos, Spain). *Journal of Human Evolution, 63*(4), 610–623. https://doi.org/10.1016/j.jhevol.2012.06.008

Parés, J. M., & Pérez-González, A. (1999). Magnetochronology and stratigraphy at Gran Dolina section, Atapuerca (Burgos, Spain). *Journal of Human Evolution, 37*(3–4), 325–342.

Parés, J. M., Pérez-González, A., Rosas, A., Benito-Calvo, A., Bermúdez de Castro, J. M., Carbonell, E., & Huguet, R. (2006). Matuyama-age lithic tools from the Sima del Elefante site, Atapuerca (northern Spain). *Journal of Human Evolution, 50*, 163–169.

Parés, J. M., Arnold, L., Duval, M., Demuro, M., Pérez-González, A., Bermúdez de Castro, J. M., Carbonell, E., & Arsuaga, J. L. (2013). Reassessing the age of Atapuerca-TD6 (Spain): New paleomagnetic results. *Journal of Archaeological Science, 40*(12), 4586–4595.

Parés, J. M., Ortega, A. I., Benito-Calvo, A., Aramburu, A., Bermúdez de Castro, J. M., Carbonell, E. (2015). Paleomagnetic constraints on the Atapuerca Karst development (N Spain). In Feinberg y Gao, J., & Calvin Alexandre, E. (Eds.), Caves and Karst across Time, edited by GSA Special Volume.

Parés, J. M., Álvarez-Posada, C., Sier, M., Moreno, D., Duval, M., Woodhead, J. D., Ortega, A. I., Campaña, I., Rosell, J., Bermúdez de Castro, J. M., & Carbonell, E. (2018). Chronology of the cave interior sediments at Gran Dolina archaeological site, Atapuerca (Spain). *Quaternary Science Reviews, 186*, 1–16.

Pérez-González, A., Aleixandre, T., Pinilla, A., Gallardo, J., Benayas, J., & Martínez, M. J. (1995). Aproximación a la estratigrafía de galería en la trinchera de la Sierra de Atapuerca (Burgos). En J. M. Bermúdez de Castro, J. L. Arsuaga, & E. Carbonell (Eds.), Evolución humana en Europa y los yacimientos de la Sierra de Atapuerca (pp. 99–122).

Pérez-González, A., Parés, J. M., Gallardo, J., Aleixandre, T., Ortega, A. I., & Pinilla, A. (1999). Geología y estratigrafía del relleno de Galería de la Sierra de Atapuerca (Burgos). In: ATAPUERCA: Ocupaciones humanas y paleoecología del yacimiento de Galería. Eds: Carbonell, E., Rosas, A., & Díez, C. 31–42.

Pérez-González, A., Parés, J. M., Carbonell, E., Aleixandre, T., Ortega, A. I., Benito-Calvo, A., & Martín-Merino, M. A. (2001). Géologie de la Sierra de Atapuerca et stratigraphie des remplissages karstiques de Galería et Dolina (Burgos, Espagne). *L'anthropologie, 105*(1), 27–43.

Reams, M. W. (1968). *Cave sediments and the geomorphic history of the Ozarks*. Washington University.

Rodríguez, J., Burjachs, F., Cuenca-Bescós, G., García, N., Van der Made, J., Pérez González, A., Blain, H. A., Expósito, I., López-García, J. M., García Antón, M., Allué, E., Cáceres, I., Huguet, R., Mosquera, M., Ollé, A., Rosell, J., Parés, J. M., Rodríuez, X. P., Díez, C., Carbonell, E. (2011). One million years of cultural evolution in a stable environment at Atapuerca (Burgos, Spain). *Quaternary Science Reviews*.

Rodríguez-Gómez, G., Rodríguez, J., Martín-González, J. T., & Goikoetxea, I. (2013). Modeling trophic resource availability for the first human settlers of Europe: The case of Atapuerca TD6. *Journal of Human Evolution, 64*(6), 645–657.

Rosas, A., Pérez-González, A., Carbonell, E., Van der Made, J., Sánchez, A., Laplana, C., Cuenca-Bescós, G., Parés, J. M., & Huguet, R. (2001). Le gisement pléistocène de la "Sima del Elefante" (Sierra de Atapuerca, Espagne). *L'anthropologie, 105*(2), 301–312.

Rosas, A., Huguet, R., Pérez-González, A., Carbonell, E., Bermúdez de Castro, J. M., Vallverdú, J., Van der Made, J., Allué, E., García, N., Martínez-Pérez, R., Rodríguez, J., Sala, R., Saladié, P., Benito-Calvo, A., Martínez-Maza, C., Bastir, M., Sánchez, A., & Parés, J. M. (2006). The "Sima del Elefante" cave site at Atapuerca (Spain). *Estudios Geológicos, 62*(1), 327–348.

Sasowsky, I. D. (2007). Clastic sediments in caves—Imperfect recorders of processes in karst. *Acta Carsologica, 36*(1), 143–149.

Shaw, T. R. (1992). History of Cave Science. Sydney Speleological Society.

Springer, G. S., & Kite, J. S. (1997b). River-derived slackwater sediments in caves along Cheat River. *West Virginia. Geomorphology, 18*(2), 91–100.

Sundborg, A. (1956). The River Klaralven, a study in fluvial processes. *Geografiska Annaler, 38*, 125–316.

Van Loon, A. J. (2009). Soft-sediment deformation structures in siliciclastic sediments: An overview. *Geologos, 15*, 3–55.

Wagner, T., Fritz, H., Stüwe, K., Nestroy, O., Rodnight, H., Hellstrom, J., & Benischke, R. (2011). Correlations of cave levels, stream terraces and planation surfaces along the River Mur—Timing of landscape evolution along the eastern margin of the Alps. *Geomorphology, 134*, 62–78.

White, W. B. (2007). Cave sediments and paleoclimate. *Journal of Cave and Karst Studies, 69*(1), 76–93.

Zazo, C., Goy, J. L., Hoyos, M. (1987). Contexto geológico y geomorfológico. In: *El hombre fósil de Ibeas y el Pleistoceno de la Sierra de Atapuerca*, edited by E. Aguirre, E. Carbonell and J. M. Bermúdez de Castro. Soria: Junta de Castilla y León.